

Normal Modes of a Spin Cycloid or Helix*

Randy S. Fishman¹, Toomas Rõõm², and Rogério de Sousa³

¹*Materials Science and Technology Division, Oak Ridge National Laboratory, Oak Ridge, Tennessee, USA*

²*National Institute of Chemical Physics and Biophysics, Akadeemia tee 23, 12618 Tallinn, Estonia and*

³*Department of Physics and Astronomy, University of Victoria, Victoria, British Columbia, Canada V8W 2Y2*

(Dated: May 2, 2022)

Although spin cycloids and helices are quite common, remarkably little is known about the normal modes of a spin cycloid or helix with finite length on a discrete lattice. Based on simple one-dimensional lattice models, we numerically evaluate the normal modes of a spin cycloid or helix produced by either Dzyaloshinskii-Moriya (DM) or competing exchange (CE) interactions. The normal modes depend on the type of interaction and on whether the nearest-neighbor exchange is antiferromagnetic (AF) or ferromagnetic (FM). In the DM case, there is only a single Goldstone mode; in the CE case, there are three. For FM exchange, the spin oscillations produced by non-Goldstone modes contain a mixture of tangential and transverse components. For the DM case, we compare our numerical results with analytic results in the continuum limit.

PACS numbers: 75.25.+z, 75.30.Ds, 78.30.-j, 75.50.Ee

Spin cycloids and helices are ubiquitous in the field of magnetism. They appear in most multiferroics^{1–3} and in many other materials like rare earths^{4,5}, intermetallics^{6–8}, and even superconductors^{9,10}. Cycloids with spins in the same plane as the ordering wavevector \mathbf{Q} and helices (also known as spirals or proper screws) with spins perpendicular to \mathbf{Q} partly satisfy neighboring exchange interactions and some competing energy like Dzyaloshinskii-Moriya (DM) or competing exchange (CE) interactions. Cycloids and helices have attracted great attention not only for their response to competing energies but also for applications based on their control with electric or magnetic fields¹¹.

The excitation spectrum of a cycloid or helix provides a dynamical “fingerprint” of the microscopic interactions and anisotropies responsible for its formation. Yet remarkably little is known about the spectrum of spin-wave (SW) modes for a cycloid or helix, especially one with a finite period on a discrete lattice. This paper studies simple one-dimensional lattice Hamiltonians for DM and CE cycloids or helices with either antiferromagnetic (AF) or ferromagnetic (FM) nearest-neighbor exchange. Our work seeks to answer several questions. Are the mode spectra and SW amplitudes different for the four cases (AF/DM, FM/DM, AF/CE, and FM/CE) considered? Which SW modes are observable by inelastic neutron scattering (INS) and which by optical spectroscopy? How

is the continuum limit approached in these four cases?

A simple one-dimensional lattice Hamiltonian for a DM cycloid is

$$\mathcal{H}_{\text{DM}} = -J_1 \sum_i \mathbf{S}_i \cdot \mathbf{S}_{i+1} - D \sum_i \mathbf{y} \cdot (\mathbf{S}_{i+1} \times \mathbf{S}_i), \quad (1)$$

where neighboring sites i and $i+1$ are separated by lattice constant a along the x axis. The DM interaction D along \mathbf{y} constrains the spins to lie in the xz plane. A helix with spins in the yz plane would be produced by a DM interaction along \mathbf{x} . A one-dimensional lattice Hamiltonian for a CE cycloid or helix is

$$\mathcal{H}_{\text{CE}} = -J_1 \sum_i \mathbf{S}_i \cdot \mathbf{S}_{i+1} - J_2 \sum_i \mathbf{S}_i \cdot \mathbf{S}_{i+2}, \quad (2)$$

where J_2 is the next-nearest-neighbor exchange coupling between sites i and $i+2$. For either sign of J_1 , the DM interaction or AF exchange $J_2 < 0$ frustrates simple AF or FM order to produce a cycloid or helix.

Using classical spins, it is easy to show that a cycloid or helix of period Ma is produced by the DM interaction D in \mathcal{H}_{DM} when

$$D = J_1 \tan(2\pi\delta). \quad (3)$$

For AF $J_1 < 0$, $\delta = p/2M$ where p is the number of 2π rotations (not counting the AF oscillations) in distance $2Ma$ and the ordering wavevector is $\mathbf{Q} = (2\pi/a)(0.5 + \delta)\mathbf{x}$. The cycloid or helix is periodic in distance Ma if p is odd (even) and M is odd (even). For FM $J_1 > 0$, $\delta = p/M$ where p is the number of 2π rotations in distance Ma and $\mathbf{Q} = (2\pi/a)\delta\mathbf{x}$.

A cycloid or helix with period Ma is also produced by the next-nearest-neighbor exchange J_2 in \mathcal{H}_{CE} when

$$J_2 = -\frac{|J_1|}{4} \sec(2\pi\delta). \quad (4)$$

For $J_1 < 0$, $\delta = p/2M$ and for $J_1 > 0$, $\delta = p/M$ as above. The ordering wavevectors \mathbf{Q} are the same as for DM interactions. Only collinear AF or FM order is possible when $|J_2| < |J_1|/4$.

*Copyright notice: This manuscript has been authored by UT-Battelle, LLC under Contract No. DE-AC05-00OR22725 with the U.S. Department of Energy. The United States Government retains and the publisher, by accepting the article for publication, acknowledges that the United States Government retains a non-exclusive, paid-up, irrevocable, world-wide license to publish or reproduce the published form of this manuscript, or allow others to do so, for United States Government purposes. The Department of Energy will provide public access to these results of federally sponsored research in accordance with the DOE Public Access Plan (<http://energy.gov/downloads/doe-public-access-plan>).

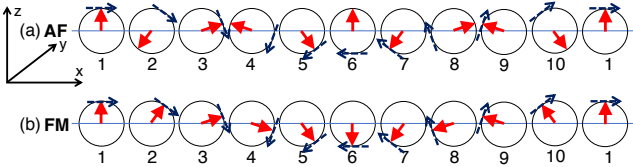


FIG. 1: (Color online) Cycloids with (a) AF or (b) FM nearest-neighbor coupling, both with $\delta = 1/10$. Spins \mathbf{S}_r are solid arrows, tangents \mathbf{t}_r are dashed arrows.

For specificity, we shall consider a cycloid with spins in the xz plane containing \mathbf{Q} . While this condition is guaranteed by the DM interaction along \mathbf{y} in \mathcal{H}_{DM} , the spin plane is not determined by the CE interactions in \mathcal{H}_{CE} . The spins can then be constrained to the xz plane by adding a small (infinitesimal) easy-plane anisotropy K along \mathbf{y} . On the other hand, a helix with spins in the yz plane perpendicular to \mathbf{Q} would be created by a DM interaction or easy-plane anisotropy along \mathbf{x} . All the numerical results below also hold for a spin helix with the appropriate rotation of the spin reference frame¹². Our new continuum-limit results for the FM/DM case are also valid for both cycloids and helices.

A classical cycloid with spins in the xz plane is given by

$$\mathbf{S}_r = S(\sin(Qra), 0, \cos(Qra)), \quad (5)$$

where S is the spin and $R = ra$ is the position of site r . Since $\mathbf{S}_{r+M} = \mathbf{S}_r$, the magnetic unit cell contains M spins with $1 \leq r \leq M$. For AF or FM interactions, cycloids with $\delta = 1/10$ are sketched in Fig.1. Notice that the tangent¹²

$$\mathbf{t}_r = (\cos(2\pi\delta r), 0, -\sin(2\pi\delta r)) \quad (6)$$

does not alternate sign with the AF modulation in Fig.1(a).

We solve for the SW modes of these two models by performing a $1/S$ expansion about the classical limit and then diagonalizing a $2M \times 2M$ equation-of-motion matrix^{13,14}. We always take $S = 5/2$. The predicted INS intensities $S(q, \omega)$ are plotted in Fig.2 for all four cases with $\delta = 1/10$. Clear signatures are exhibited by the spectra produced by DM and CE cycloids and by AF and FM interactions. For CE cycloids, the SW modes always fall within the first structural Brillouin zone between $H = 0$ and 1, as can be seen from the SW frequencies plotted as dashed curves. For DM cycloids, the SW branches extend beyond the first Brillouin zone. For example, three SW branches arise from $H = \pm 1/10$ and $H = 0$ for the DM/FM case in Fig.2(b).

The normal modes evaluated at wavevector $H = m\delta$ (integer m) may appear in optical measurements since zone folding maps those wavevectors onto $q = 0$. To understand the different mode spectra in our four cases, we plot the SW dispersions versus wavevector q in Fig.3. Any normal mode crossed by two SW branches is doubly degenerate¹⁵.

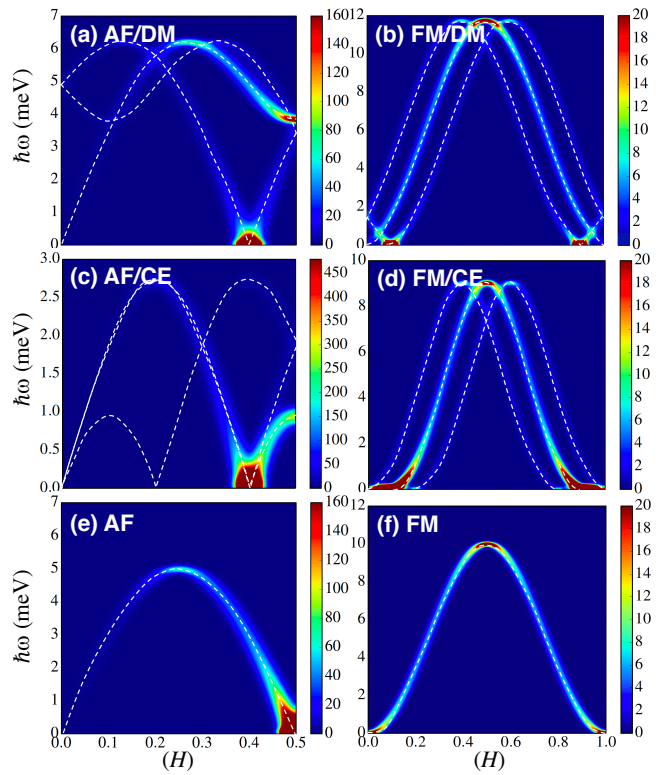


FIG. 2: (Color online) The INS intensity $S(q, \omega)$ with $q = 2\pi H/a$ and $\delta = 1/10$ for (a, b) DM cycloids and (c, d) CE cycloids with either (a, c) AF or (b, d) FM exchange $|J_1| = 1$ meV. For reference, the INS intensities for simple AF or FMs with $D = 0$ and $J_2 = 0$ are given in (e) and (f). Frequencies of modes with significant intensity are drawn as dashed curves.

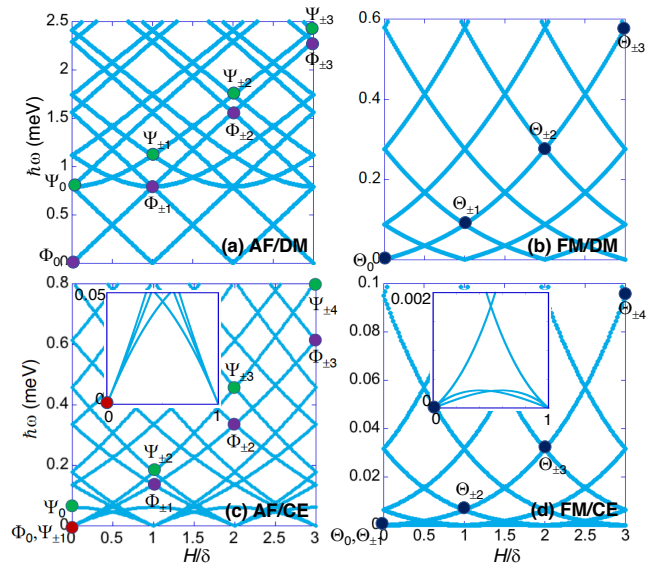


FIG. 3: (Color online) The SW frequencies versus H/δ for (a, b) DM cycloids and (c, d) CE cycloids with either (a, c) AF or (b, d) FM exchange $|J_1| = 1$ meV. In all cases, $\delta = 1/40$.

For AF interactions, we obtain two classes of modes labeled $\Phi_{\pm n}$ and $\Psi_{\pm n}$ (doubly degenerate for $n > 0$). In the AF/DM case, the single Goldstone mode Φ_0 corresponds to a uniform spin rotation about \mathbf{y} . The mode spectrum in Fig.3(a) is close to the spectrum predicted by de Sousa and Moore¹⁶ in the continuum limit with $\hbar\omega(\Phi_{\pm n}) = 2S|D|n$ and $\hbar\omega(\Psi_{\pm n}) = 2S|D|\sqrt{1+n^2}$. In the AF/CE case, the three Goldstone modes are Φ_0 and $\Psi_{\pm 1}$. Their three-fold splitting away from $H = 0$ is plotted in the inset to Fig.3(c) and can also be seen in Fig.2(c). Goldstone modes $\Psi_{\pm 1}$ are associated with rotations out of the xz plane, assuming that the easy-plane anisotropy K vanishes. Of course, this rotation costs energy in the AF/DM case.

For FM interactions, we obtain only one class of modes labeled $\Theta_{\pm n}$ (doubly degenerate for $n > 0$). In the FM/DM case, the single Goldstone mode Θ_0 again corresponds to a uniform spin rotation about \mathbf{y} . In the continuum limit of the FM/DM case, we find that $\hbar\omega(\Theta_{\pm n}) = S(D^2/J)n\sqrt{1+n^2}$. In the FM/CE case, the three Goldstone modes are Θ_0 and $\Theta_{\pm 1}$ with the three-fold splitting plotted in the inset to Fig.3(d). As in the AF/CE, the extra Goldstone modes are associated with rotations of the spin state out of the xz plane. In all four cases, the Goldstone modes are “massless,” which means that the dispersion is linear near $H = 0$.

The spin oscillation $\Delta\mathbf{S}_r^{(n)}(\mathbf{q}, t)$ at site r produced by SW mode n with wavevector \mathbf{q} is generally given by^{14,17}

$$\Delta\mathbf{S}_r^{(n)}(\mathbf{q}, t) = 2\sqrt{N} \operatorname{Re} \left\{ e^{-i\omega_n t} \delta\mathbf{S}_r(n, \mathbf{q}) \right\}, \quad (7)$$

$$\delta\mathbf{S}_r(n, \mathbf{q}) = \langle 0 | \mathbf{S}_r | n, \mathbf{q} \rangle, \quad (8)$$

where $|0\rangle$ is the ground state, $|n, \mathbf{q}\rangle$ is an excited state containing a single SW with energy $\omega_n(\mathbf{q})$ at wavevector \mathbf{q} , and \mathbf{S}_r is the quantum spin operator at site r . Like the SW frequency $\omega_n(\mathbf{q})$, the SW amplitude $\delta\mathbf{S}_r(n, \mathbf{q})$ is the same at wavevectors $\mathbf{q} = 0$ and $\mathbf{q} = \mathbf{Q}$.

A close examination of the SW amplitudes for DM and CE cycloids with AF or FM interactions reveals that

$$\delta\mathbf{S}_r(\Phi_{\pm n}) = \left\{ \xi_1^{(n)} \mathbf{t}_r (-1)^r - i \xi_2^{(n)} \mathbf{y} \right\} e^{\pm 2\pi i n \delta r} \text{ (AF)}, \quad (9)$$

$$\delta\mathbf{S}_r(\Psi_{\pm n}) = \left\{ \rho_1^{(n)} \mathbf{y} (-1)^r + i \rho_2^{(n)} \mathbf{t}_r \right\} e^{\pm 2\pi i n \delta r} \text{ (AF)}, \quad (10)$$

$$\delta\mathbf{S}_r(\Theta_{\pm n}) = \left\{ \gamma_1^{(n)} \mathbf{t}_r - i \gamma_2^{(n)} \mathbf{y} \right\} e^{\pm 2\pi i n \delta r} \text{ (FM)}, \quad (11)$$

for either $q = 0$ or $q = Q$. In each case, the real and positive coefficients are the same for the degenerate $\pm n$ modes and are normalized by $\xi_1^{(n)2} + \xi_2^{(n)2} = 1$, $\rho_1^{(n)2} + \rho_2^{(n)2} = 1$, and $\gamma_1^{(n)2} + \gamma_2^{(n)2} = 1$. The complex factors in the brackets imply that the tangential and transverse spin oscillations are out of phase. These factors switch sign when the helicity of the cycloid is reversed.

The SW amplitudes for the Goldstone modes are purely transverse (out of the cycloidal plane) or tangential (in the cycloidal plane). For AF interactions,

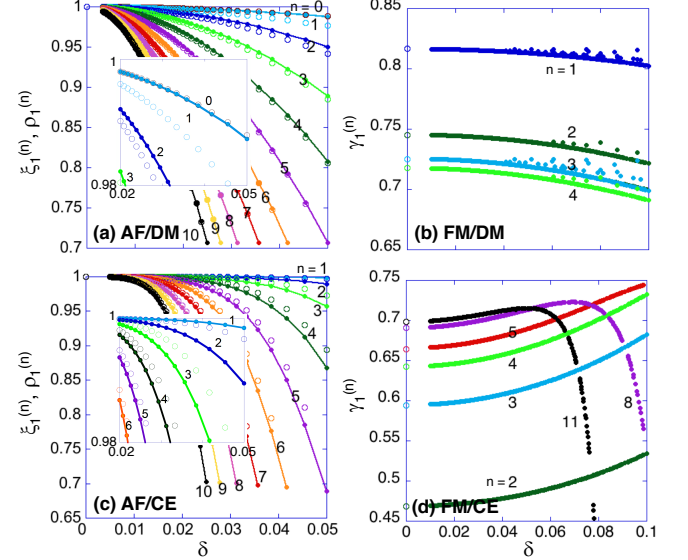


FIG. 4: (Color online) Coefficients $\xi_1^{(n)}$ and $\rho_1^{(n)}$ (AF) or $\gamma_1^{(n)}$ (FM) versus δ for the same four cases as in Fig.2. In (a) and (c), closed circles give $\xi_1^{(n)}$ and open circles give $\rho_1^{(n)}$. Points at $\delta = 0$ are exact results in the continuum limit for the FM/DM case and extrapolations for the FM/CE case. Goldstone modes not shown.

$\delta\mathbf{S}_r(\Phi_0) = \mathbf{t}_r(-1)^r$ in both the DM and CE cases. In the AF/CE case, $\delta\mathbf{S}_r(\Psi_{\pm 1}) = \exp(\pm 2\pi i \delta r)(-1)^r \mathbf{y}$. For FM interactions, $\delta\mathbf{S}_r(\Theta_0) = \mathbf{t}_r$ in both the DM and CE cases. In the FM/CE case, $\delta\mathbf{S}_r(\Theta_{\pm 1}) = \exp(\pm 2\pi i \delta r) \mathbf{y}$. Although not a Goldstone mode, the SW amplitude $\delta\mathbf{S}_r(\Psi_0) = (-1)^r \mathbf{y}$ of the AF/CE mode Ψ_0 is purely transverse but out of phase with the cycloid.

While even and odd M were handled differently for AF interactions, physical results only depend on the wavevector parameter δ . The amplitude coefficients are plotted versus δ in Fig.4. In either the AF/DM or AF/CE case, $\xi_1^{(n)}$ and $\rho_1^{(n)}$ approach 1 for all n in the continuum limit $\delta \rightarrow 0$. All the SW amplitudes become purely tangential or transverse as $\delta \rightarrow 0$ but coefficients with larger n converge much more slowly than for smaller n . Figures 4(a) and (c) plot $\xi_1^{(n)}$ and $\rho_1^{(n)}$ as closed and open circles, respectively. For larger n , $\xi_1^{(n)}$ and $\rho_1^{(n)}$ are quite close, but deviations can be seen for smaller n away from $\delta = 0$.

For FM interactions, the behavior of the coefficients is more complex. While $\gamma_1^{(n)} \rightarrow 1/\sqrt{2}$ as $\delta \rightarrow 0$ and $n \rightarrow \infty$ in both the FM/DM and FM/CE cases, $\gamma_1^{(n)}$ have higher (FM/DM) or lower (FM/CE) limits for smaller $n > 0$. Recall that $\gamma_1^{(1)} = 0$ for the FM/CE case while $\gamma_1^{(0)} = 1$ for both FM cases. In the continuum limit of the FM/DM case, we have proven that $\gamma_1^{(n)} \rightarrow \sqrt{(1+n^2)/(1+2n^2)}$. Although we lack a rigorous proof, we numerically find that $\gamma_1^{(n)} \rightarrow |n^2 - 1|/\sqrt{2n^4 + 2n^2 + 1}$ in the continuum limit of the FM/CE case. So non-Goldstone modes always mix tangential and transverse components for FM interactions.

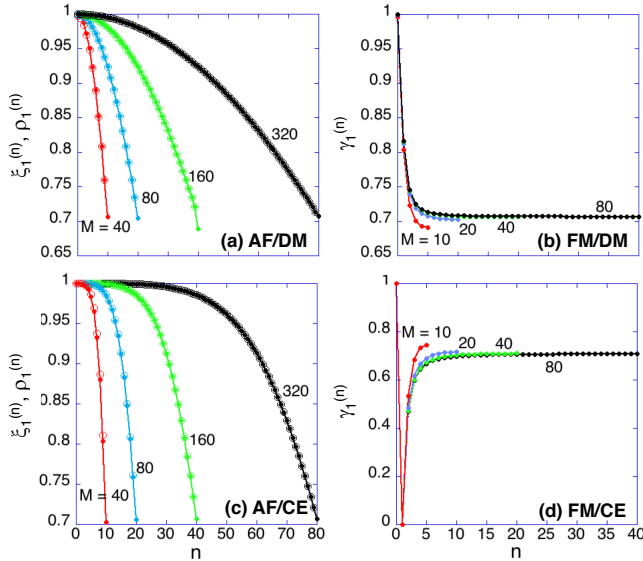


FIG. 5: (Color online) Coefficients $\xi_1^{(n)}$ and $\rho_1^{(n)}$ (AF) or $\gamma_1^{(n)}$ (FM) versus mode index n for $\delta = 1/M$ and the same four cases as in Fig.2. In (a) and (c), closed circles give $\xi_1^{(n)}$ and open circles give $\rho_1^{(n)}$. The maximum n is $M/4$ for AF interactions and $M/2$ for FM interactions.

Another way to look at these results is by plotting the coefficients versus n for a fixed $\delta = 1/M$ in Fig.5. For AF interactions, the coefficients quickly fall off from their asymptotic $\delta \rightarrow 0$ limits of $\xi_1^{(n)} = 1$ and $\rho_1^{(n)} = 1$ with increasing n . As in Fig.4, the results for $\xi_1^{(n)}$ (closed circles) and $\rho_1^{(n)}$ (open circles) are very close. Figures 4 and 5 suggest that for the maximum $n = M/4$, $\xi_1^{(n)}$ and $\rho_1^{(n)}$ approach $1/\sqrt{2}$ as M increases. In the FM/DM case, $\gamma_1^{(n)}$ falls off monotonically with n for all M and analytic results in the continuum limit are indistinguishable from numerical results for $M = 80$. In the FM/CE case, $\gamma_1^{(n)}$ increases with n starting with $\gamma_1^{(1)} = 0$. In both FM cases, $\gamma_1^{(n)}$ remains fairly constant as a function of n beyond $n = 10$ or so and approaches $1/\sqrt{2}$ for large M .

What do these results imply about the observability of the SW modes? The contribution of mode n to the spectral weight $S_{\alpha\alpha}(Q, \omega_n)$ is proportional to¹⁴

$$\left| \sum_{r=1}^M e^{-iQra} \delta S_{r\alpha}(n) \right|^2. \quad (12)$$

Using Eqs. (9-11), it is straightforward to show that the three modes Φ_0 ($\alpha = x$ or z), Ψ_1 ($\alpha = y$), and Φ_2 ($\alpha = x$ or y) contribute for AF interactions while the three modes Θ_0 ($\alpha = x$ or z), Θ_1 ($\alpha = y$), and Θ_2 ($\alpha = x$ or y) contribute for FM interactions. These modes are responsible for the INS intensity¹⁸ $S(q, \omega) = S_{yy}(q, \omega) + S_{zz}(q, \omega)$ plotted in Fig.1.

The purely magnetic contribution of mode n to the

optical absorption is proportional to¹⁴

$$\omega_n \left| \sum_{r=1}^M \mathbf{h} \cdot \delta \mathbf{S}_r(n) \right|^2 = \frac{\omega_n}{4\mu_B^2} \left| \langle 0 | \mathbf{h} \cdot \mathbf{M} | n, q = 0 \rangle \right|^2, \quad (13)$$

where \mathbf{h} is the magnetic polarization of light and $\mathbf{M} = 2\mu_B \sum_{r=1}^M \mathbf{S}_r$ is the magnetization per unit cell. This is nonzero for $\Psi_{\pm 1}$ in the AF/DM case and for $\Theta_{\pm 1}$ in the FM/DM case, both when $\mathbf{h} = \mathbf{x}$ or \mathbf{z} . So for nonzero δ , optical spectroscopy will detect two modes ($\Psi_{\pm 1}$) in the AF/DM case, two ($\Theta_{\pm 1}$) in the FM/DM case, and none in the CE cases. Only the FM/DM $\Theta_{\pm 1}$ modes remain optically active as $\delta \rightarrow 0$.

Notice that different parts of $\delta \mathbf{S}_r(n)$ contribute to the INS intensity and to the optical absorption. For the AF/DM $\Psi_{\pm 1}$ and FM/DM $\Theta_{\pm 1}$ modes, the tangential parts of $\delta \mathbf{S}_r(n)$ contribute to the optical absorption while the transverse parts contribute to the INS intensity.

Although few modes are optically active for the simple Hamiltonians \mathcal{H}_{DM} and \mathcal{H}_{CE} , several physical perturbations can activate other modes¹⁹. For the AF/DM compound BiFeO₃, easy-axis anisotropy²⁰ makes $\xi_2^{(0)}$ nonzero so that Φ_0 (no longer a Goldstone mode) becomes optically active for $\mathbf{h} = \mathbf{y}$. Hybridization with Φ_0 then activates²¹ $\Phi_{\pm 2}$, also for $\mathbf{h} = \mathbf{y}$. The alternating tilt of the cycloid²² on neighboring hexagonal planes mixes transverse and tangential components, thereby activating²³ Ψ_0 and $\Phi_{\pm 1}$. Consequently, eight modes (four accounting for their degeneracies and excluding the low-frequency mode Φ_0) appear in the Raman²⁴ and THz²⁵ spectra of BiFeO₃ in zero field. Due to hybridization, a magnetic field activates the complete mode spectrum²⁶.

How do other well-known materials with cycloidal or helical states fall into the four cases considered here? With helical AF2 and cycloidal AF5 states created by long-range competing AF interactions²⁷, Co-doped²⁸ MnWO₄ falls into the AF/CE class. Although itinerant⁶, MnSi is a member of the FM/DM family²⁹ and its inelastic neutron-scattering spectra³⁰ agrees with Fig.2(b). Of the three observed modes in MnSi, only the central Θ_1 mode is predicted to be optically active. A rare member of the FM/CE class, Sr₃Fe₂O₇ has a helical state produced by the competition between FM nearest-neighbor double exchange and AF next-nearest neighbor exchange³¹.

To summarize, we have evaluated the normal modes of a spin cycloid or helix¹² produced by either DM or CE interactions and for either AF or FM nearest-neighbor exchange coupling. In the continuum limit for AF exchange, the SW amplitudes for all modes are either purely tangential or transverse. But for FM exchange, the SW amplitudes for all modes except the Goldstone modes contain both tangential and transverse components, even in the continuum limit. Whereas the mode spectrum for DM interactions contains only one Goldstone mode, the mode spectrum for CE interactions contains three Goldstone modes. Our results explain why

only a subset of these modes are observable using neutron scattering or optical absorption.

Research by RF sponsored by the U.S. Department of Energy, Office of Basic Energy Sciences, Materials Sciences and Engineering Division. TR would like to acknowledge support from the Estonian Ministry of Education and Research with institutional research funding IUT23-3, and the European Regional Development Fund Project No. TK134. RdS acknowledges financial support from NSERC (Canada) through its Discovery program (RGPIN-2015-03938).

cation and Research with institutional research funding IUT23-3, and the European Regional Development Fund Project No. TK134. RdS acknowledges financial support from NSERC (Canada) through its Discovery program (RGPIN-2015-03938).

¹ Maxim Mostovoy. Ferroelectricity in spiral magnets. *Phys. Rev. Lett.*, 96:067601, Feb 2006.

² Sang-Wook Cheong and Maxim Mostovoy. Multiferroics: a magnetic twist for ferroelectricity. *Nature Materials*, 6:13 EP –, 01 2007.

³ Yoshinori Tokura, Shinichiro Seki, and Naoto Nagaosa. Multiferroics of spin origin. *Reports on Progress in Physics*, 77(7):076501, 2014.

⁴ R. J. Elliott. Phenomenological discussion of magnetic ordering in the heavy rare-earth metals. *Phys. Rev.*, 124:346–353, Oct 1961.

⁵ Jens Jensen and Allan R. Mackintosh. *Rare Earth Magnetism: Structures and Excitations*. Clarendon Press, Oxford, 1991.

⁶ Y. Ishikawa, K. Tajima, D. Bloch, and M. Roth. Helical spin structure in manganese silicide MnSi. *Solid State Communications*, 19(6):525 – 528, 1976.

⁷ N. J. Curro, P. C. Hammel, P. G. Pagliuso, J. L. Sarrao, J. D. Thompson, and Z. Fisk. Evidence for spiral magnetic order in the heavy fermion material CeRhIn₅. *Phys. Rev. B*, 62:R6100–R6103, Sep 2000.

⁸ S. Nandi, A. Kreyssig, Y. Lee, Yogesh Singh, J. W. Kim, D. C. Johnston, B. N. Harmon, and A. I. Goldman. Magnetic ordering in EuRh₂As₂ studied by x-ray resonant magnetic scattering. *Phys. Rev. B*, 79:100407, Mar 2009.

⁹ J. W. Lynn, S. Skanthakumar, Q. Huang, S. K. Sinha, Z. Hossain, L. C. Gupta, R. Nagarajan, and C. Godart. Magnetic order and crystal structure in the superconducting RNi₂B₂C materials. *Phys. Rev. B*, 55:6584–6598, Mar 1997.

¹⁰ Wei Bao, Y. Qiu, Q. Huang, M. A. Green, P. Zajdel, M. R. Fitzsimmons, M. Zhernenkov, S. Chang, Minghu Fang, B. Qian, E. K. Vehstedt, Jinhua Yang, H. M. Pham, L. Spinu, and Z. Q. Mao. Tunable ($\delta\pi$, $\delta\pi$)-type antiferromagnetic order in α -Fe(Te,Se) superconductors. *Phys. Rev. Lett.*, 102:247001, Jun 2009.

¹¹ R. Ramesh and Nicola A. Spaldin. Multiferroics: progress and prospects in thin films. *Nature Materials*, 6:21 EP –, 01 2007.

¹² For a helix (also known as a spiral or proper screw) propagating along \mathbf{x} , the spins would have values

$$\mathbf{S}_r = S(0, \sin(Qra), \cos(Qra)) \quad (14)$$

with the tangent

$$\mathbf{t}_r = (0, \cos(2\pi\delta r), -\sin(2\pi\delta r)). \quad (15)$$

The transverse direction in Eqs.(9-11) would then be \mathbf{x} instead of \mathbf{y} .

¹³ J. T. Haraldsen and R. S. Fishman. Spin rotation technique for non-collinear magnetic systems: application to the generalized Villain model. *Journal of Physics: Condensed Matter*, 21(21):216001, 2009.

¹⁴ Randy S. Fishman, Jaime Fernandez-Baca, and Toomas Rõõm. *Spin-Wave Theory and its Applications to Neutron Scattering and THz Spectroscopy*. Morgan and Claypool Publishers, San Rafael, 2018.

¹⁵ In Fig.3(a), only one SW branch crosses Ψ_0 because the frequencies of $\Phi_{\pm 1}$ are slightly lower than that of Ψ_0 when $\delta > 0$.

¹⁶ Rogerio de Sousa and Joel E. Moore. Optical coupling to spin waves in the cycloidal multiferroic BiFeO₃. *Phys. Rev. B*, 77:012406, Jan 2008.

¹⁷ Claude Cohen-Tannoudjii, Bernard Diu, and Franck Laloë. *Quantum Mechanics*. John Wiley & Sons, New York, 2005.

¹⁸ Inelastic neutron scattering measures

$$\begin{aligned} S(q, \omega) &= \sum_{\alpha, \beta} \left\{ \delta_{\alpha\beta} - q_\alpha q_\beta / q^2 \right\} S_{\alpha\beta}(q, \omega) \\ &= S_{yy}(q, \omega) + S_{zz}(q, \omega) \end{aligned}$$

for \mathbf{q} along \mathbf{x} .

¹⁹ For odd M and AF exchange, modes $\Phi_{\pm(2n+1)}$ and $\Psi_{\pm 2n}$ are missing from the spectrum because $\mathbf{t}_M = -\mathbf{x}$ differs from $\mathbf{t}_0 = \mathbf{x}$ and $\delta\mathbf{S}_M \neq \mathbf{S}_0$. Consequently, those modes only become observable under some perturbation that breaks the invariance of the system when translated by Ma with odd M . One possibility is the dimerization of the lattice with period $2a$. Another is the AF coupling between adjacent hexagonal planes but FM coupling within each plane, as for BiFeO₃²⁰. With FM exchange, $\mathbf{t}_M = \mathbf{x}$ for either even or odd M so the complete spectrum of modes $\Theta_{\pm n}$ always appears.

²⁰ I. Sosnowska and A. K. Zvezdin. Origin of the long period magnetic ordering in BiFeO₃. *Journal of Magnetism and Magnetic Materials*, 140-144:167 – 168, 1995. International Conference on Magnetism.

²¹ Randy S. Fishman, Nobuo Furukawa, Jason T. Haraldsen, Masaaki Matsuda, and Shin Miyahara. Identifying the spectroscopic modes of multiferroic BiFeO₃. *Phys. Rev. B*, 86:220402, Dec 2012.

²² A. M. Kadomtseva, A. K. Zvezdin, Yu. F. Popov, A. P. Pyatakov, and G. P. Vorob'ev. Space-time parity violation and magnetoelectric interactions in antiferromagnets. *Journal of Experimental and Theoretical Physics Letters*, 79(11):571–581, Jun 2004.

²³ Randy S. Fishman, Jason T. Haraldsen, Nobuo Furukawa, and Shin Miyahara. Spin state and spectroscopic modes of multiferroic BiFeO₃. *Phys. Rev. B*, 87:134416, Apr 2013.

²⁴ M. Cazayous, Y. Gallais, A. Sacuto, R. de Sousa, D. Lebeugle, and D. Colson. Possible observation of cycloidal electromagnons in BiFeO₃. *Phys. Rev. Lett.*, 101:037601, Jul 2008.

²⁵ D. Talbayev, S. A. Trugman, Seongsu Lee, Hee Taek Yi, S.-W. Cheong, and A. J. Taylor. Long-wavelength magnetic and magnetoelectric excitations in the ferroelectric

antiferromagnet BiFeO_3 . *Phys. Rev. B*, 83:094403, Mar 2011.

²⁶ U. Nagel, Randy S. Fishman, T. Katuwal, H. Engelkamp, D. Talbayev, Hee Taek Yi, S.-W. Cheong, and T. Rööm. Terahertz spectroscopy of spin waves in multiferroic BiFeO_3 in high magnetic fields. *Phys. Rev. Lett.*, 110:257201, Jun 2013.

²⁷ A. H. Arkenbout, T. T. M. Palstra, T. Siegrist, and T. Kimura. Ferroelectricity in the cycloidal spiral magnetic phase of MnWO_4 . *Phys. Rev. B*, 74(18):184431, 2006.

²⁸ Feng Ye, Songxue Chi, Jaime A. Fernandez-Baca, Huibo Cao, K.-C. Liang, Yaqi Wang, Bernd Lorenz, and C. W. Chu. Magnetic order and spin-flop transitions in the cobalt-doped multiferroic $\text{Mn}_{1-x}\text{Co}_x\text{WO}_4$. *Phys. Rev. B*, 86:094429, Sep 2012.

²⁹ P. Bak and M. H. Jensen. Theory of helical magnetic structures and phase transitions in MnSi and FeGe . *Journal of Physics C: Solid State Physics*, 13(31):L881, 1980.

³⁰ M. Kugler, G. Brandl, J. Waizner, M. Janoschek, R. Georgii, A. Bauer, K. Seemann, A. Rosch, C. Pfleiderer, P. Böni, and M. Garst. Band structure of helimagnons in MnSi resolved by inelastic neutron scattering. *Phys. Rev. Lett.*, 115:097203, Aug 2015.

³¹ J.-H. Kim, Anil Jain, M. Reehuis, G. Khaliullin, D. C. Peets, C. Ulrich, J. T. Park, E. Faulhaber, A. Hoser, H. C. Walker, D. T. Adroja, A. C. Walters, D. S. Inosov, A. Maljuk, and B. Keimer. Competing exchange interactions on the verge of a metal-insulator transition in the two-dimensional spiral magnet $\text{Sr}_3\text{Fe}_2\text{O}_7$. *Phys. Rev. Lett.*, 113:147206, Oct 2014.